Unraveling the Photogenerated Electron Localization on the Defect-free $CH_3NH_3PbI_3$(001) Surfaces: Understanding and Implications from a First-Principles Study

Yunxuan Ding, Yujie Shen, Chao Peng, Meilan Huang and P. Hu**

School of Chemistry and Chemical Engineering, The Queen's University of Belfast, Belfast, BT9 5AG, UK.

ABSTRACT: The localization of photogenerated electrons in photovoltaic and photocatalytic materials is crucial for reducing the electron-hole recombination rate. Here, the photogenerated electron localization is systematically investigated on the $CH_3NH_3PbI_3$ ($MAPbI_3$) perovskite using first-principles calculations. It is found that under vacuum conditions, the photogenerated electron is delocalized in the $MAPbI_3$ bulk as well as on the stochiometric $MAPbI_3$(001) surface with the CH_3NH_3I (MAI) termination, while it is trapped on the defect-free PbI_2-terminated surface. Our *ab-initio* molecular dynamics simulations reveal that the introduction of solutions will prompt the formation of localized electronic states. The photogenerated electron is discovered to be localized on both the MAI and PbI_2 terminated surfaces in the presence of solutions with different

concentrations HI from the pure water to the saturated solution. We demonstrate that the Pb-I bond weakening or breaking resulting in an unsaturated coordination of a Pb site is the prerequisite to trap the photogenerated electron.

TOC GRAPHICS

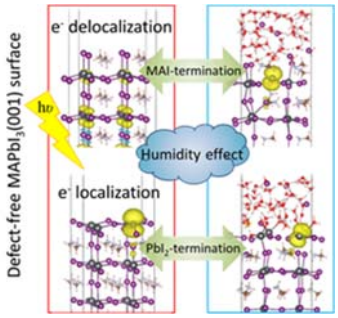

Hybrid organic−inorganic perovskite solar cells have been recognized as a new generation of highly promising materials for photovoltaic applications[1-3]. Emerging as a light harvester in the dye-sensitized solar cells, it shows ever-promising power conversion efficiency (PCE) growing from 3.8 % to 25.2% in recent years[4-9]. As one of the typical metal-halide perovskites, the $MAPbI_3$ perovskite has attracted great attention due to its excellent properties, such as a strong photoabsorption coefficient[10], an optimal band gap[11], a high charge-carrier mobility[12], a long carrier diffusion length[13-14], and a weak exciton binding energy[15]. Recently, it was also discovered that the $MAPbI_3$ perovskites also show extraordinary performances on several photocatalytic reactions, such as hydrogen evolution reaction[16-18] and carbon dioxide reduction[19-21].

However, the understanding of the high photovoltaic efficiency and the high photocatalytic performance of $MAPbI_3$ perovskites falls much short of expectation. Recently, strong evidence that the charge localization is key in photocatalytic/photovoltaic systems has emerged in the

literature[22-24]. Our group previously investigated the oxygen evolution reaction (OER) in the TiO_2 system and found that the concentration of the photogenerated hole (C_{h+}) dramatically affects the activity of OER. The low concentration of photogenerated holes C_{h+} was the main obstacle to the low photocatalytic OER efficiency in TiO_2[24-25]. Consequently, one can suggest that the high photocatalytic and high photovoltaic performance of $MAPbI_3$ perovskites may be attributed to their low electron-hole recombination rate and long excited-state lifetime[26]. Long, Prezhdo and co-workers reported that the charge recombination was sensitive to the grain boundaries and dopants, and the grain boundaries significantly enhanced the electron-hole coupling[27-28]. They also revealed that the localization of the electronic states can decrease electron-hole interactions and prolong the excited-state lifetime[29]. Specifically, the overlap between the localized electrons and holes may be smaller than that of delocalized states, thus reducing the electron-hole interaction, and the weaker electron-hole coupling would lead to slower nonradiative recombination. This means that the localization of the photogenerated electrons/holes would enhance the photocatalytic and photovoltaic efficiency; a good separation of the photogenerated electrons and holes is very desirable[30-32]. However, how charges are localized in the system of $MAPbI_3$ perovskites need to be further investigated.

Regarding the hole localization or hole-trapping, in our previous work, we discovered that an I dimer can catch a photogenerated hole both in the bulk[33] and on surfaces of $MAPbI_3$ perovskite[34]. Janáky and co-workers observed holes trapped at the iodide site, following by the iodide gradually expelled from the mix halide film as the iodine and/or triiodide ion[35]. With respect to the localization of photogenerated electrons, recent studies have shown that defects in the perovskites can help trapping electrons. Uratani et al. reported evidence of the presence of surface defects leading to trapping electrons[36]. The halide vacancy is one of the most common defects and several

studies revealed that the iodine and bromine vacancies resulted in the formation of charge trapping[37-41].

Despite of these progresses, the localization of the photogenerated electrons without defects remains elusive. For an excellent photovoltaic-photocatalytic material, a fast charge migration in the material is essential in addition to the good electron-hole separation and the charge localization. If the localized electron is always associated with a defect or defects, the electron may be trapped too deeply and thus the migration of the trapped electron will be limited because the defect diffusion is usually not easy. Consequently, the trapped electron might stay with the defect and might not be readily accessed by photovoltaic-photocatalytic applications. In addition, the humidity effect, i.e. the presence of water molecules[42-44], on the performance of $MAPbI_3$ perovskite is a hotly debated topic. One school of thought was that the performance of perovskite solar cells degrades under humid conditions[45-46], and the other reported that the moisture environments increase their performances[26, 47]. Therefore, it is necessary to answer the following questions: (i) Can the electron be trapped on the $MAPbI_3$ perovskite without defects? (ii) How would different terminated surfaces of the $MAPbI_3$ perovskite affect the localization of the photogenerated electron? (iii) Considering some photocatalytic reactions of the $MAPbI_3$ occurred in the aqueous solution as well as the humidity effect on their performances, what influence would the solution, or environmental molecules in general, bring to the electron trapping?

In this work, we investigate the electronic properties of bulk of $MAPbI_3$, MAI and PbI_2 terminated surfaces without defects using density functional theory (DFT) calculations. We find that in a vacuum condition, the electron is delocalized in the bulk as well as on the MAI terminated surface, while an electron-trapped state on the PbI_2 terminated surface without defects can be located. Our *ab-initio* molecular dynamics (AIMD) simulations show that in the presence of a

liquid phase, both the terminated surfaces can trap the electrons. The origin of the localized electronic state is identified, and the understanding and implications of these results are discussed.

We began by investigating the possibility of the localized electronic state in the bulk of $MAPbI_3$. To identify the trapped electronic state, it is crucial to create a slight structural perturbation to break the symmetry of the structure and then fully relax the structure so as to prompt the electron localization, an effective approach used in our previous work[24, 33]. The optimized structures of the neutral bulk and the bulk with an extra electron are shown in Figure 1(a) and (b), respectively. With no surprise, the electron is found to be delocalized in the bulk with the spin charges mainly distributed among the Pb atoms. As expected, the introduction of the extra electron indeed results in a slight change of the structure. The average Pb-I bond length of the bulk of $MAPbI_3$ changes from 3.16 Å to 3.21 Å, indicating a structural distortion. However, this structure distortion is still not enough for the electron localization (see more discussion below). The DOS calculations also show clearly that no polaron peak exists between the valence band maximum (VBM) and the conduction band minimum (CBM) (Figure S1), indicating the absence of electron localization.

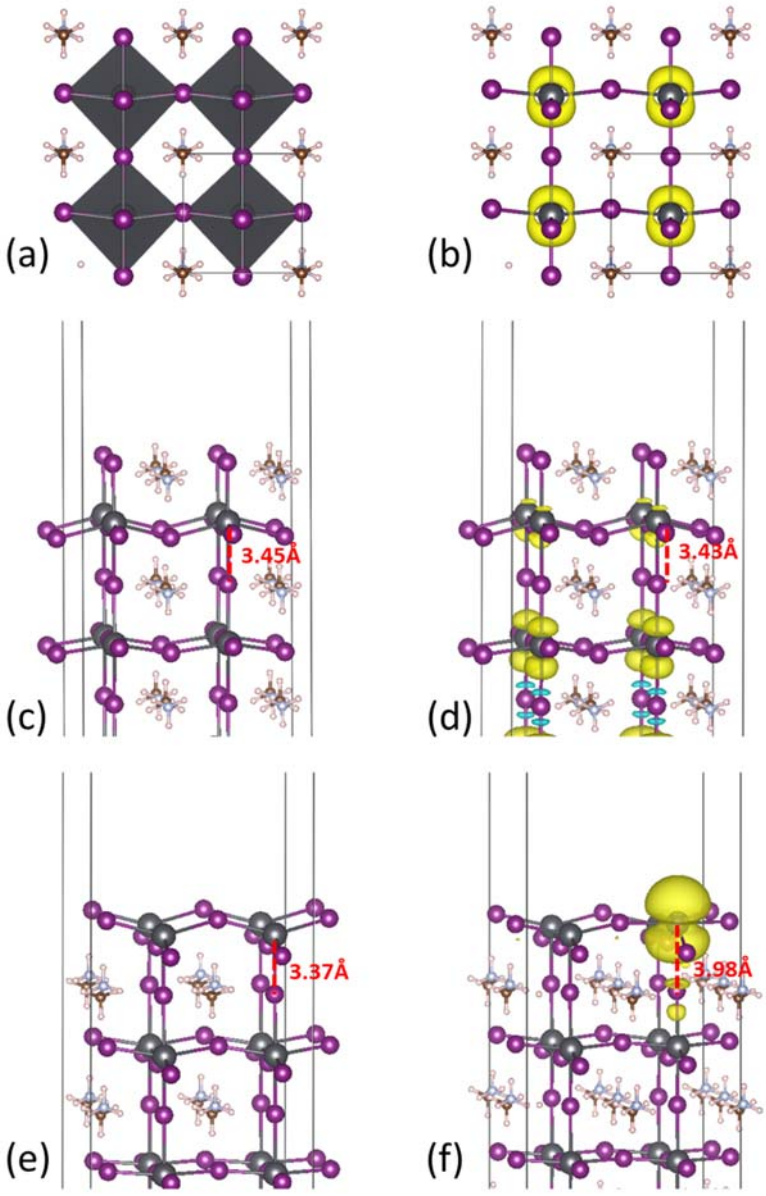

Figure 1. Geometric structures and spin densities of the cubic phase unit cell ((a), (b)), the MAI-terminated surface ((c), (d)), and the PbI2-terminated surface ((e), (f)). The systems of (a), (c) and (e) are neutral, while those of (b), (d) and (f) have an extra electron in each unit. The iso-value is 0.005 e/Å^3 for (b), 0.0005 e/Å^3 for (d), and 0.001 e/Å^3 for (f). Black: Pb; purple: I; white: H; brown: C; silver: N. This color scheme is used throughout the paper. The characteristic distance is marked by the dash line with its value beside.

To further explore the reason of the high photocatalytic/photovoltaic efficiency of $MAPbI_3$, the localization of an extra electron on the $MAPbI_3$(001) surface was systematically investigated. It has two possible terminations, i.e. MAI-terminated and PbI_2-terminated surfaces, as shown in Figure 1. Our calculations show, interestingly, that the excess electron can be trapped on the PbI_2 terminated surface (Figure 1(f)) with an energy gain of 0.35 eV compared to the delocalized electronic state. In other words, on the defect-free PbI_2 terminated surface, the electron localization is energetically more favored than the electron delocalization. In contrast, the electron is found to be delocalized on the MAI terminated surface (Figure 1(d)). Furthermore, the characteristic distance, which is defined as the bond length between the Pb atom in the first PbI_2 layer and the I atom below (marked in Figure 1), remains the same on the MAI terminated surface, while it is changed from 3.37 Å to 3.98 Å on the PbI_2 terminated surface after adding an extra electron. The DOS calculations also reveal that there is a polaron peak in the band gap on the PbI_2 terminated surface (Figure 2(a)). Specifically, the projected density of states (PDOS) demonstrate that the electron is mainly trapped on the p orbitals of the Pb atom (Figure S2). These results imply that the Pb atom is activated after the localization of the electron. In contrast, in the MAI termination, although the Fermi level is shifted due to the introduction of the electron, there is no polaron peak in the band gap (Figure 2(b)), indicating the delocalization of the electron in the system. This means that the MAI terminated surface is unable to trap the electron without help of environmental molecules, which is discussed later.

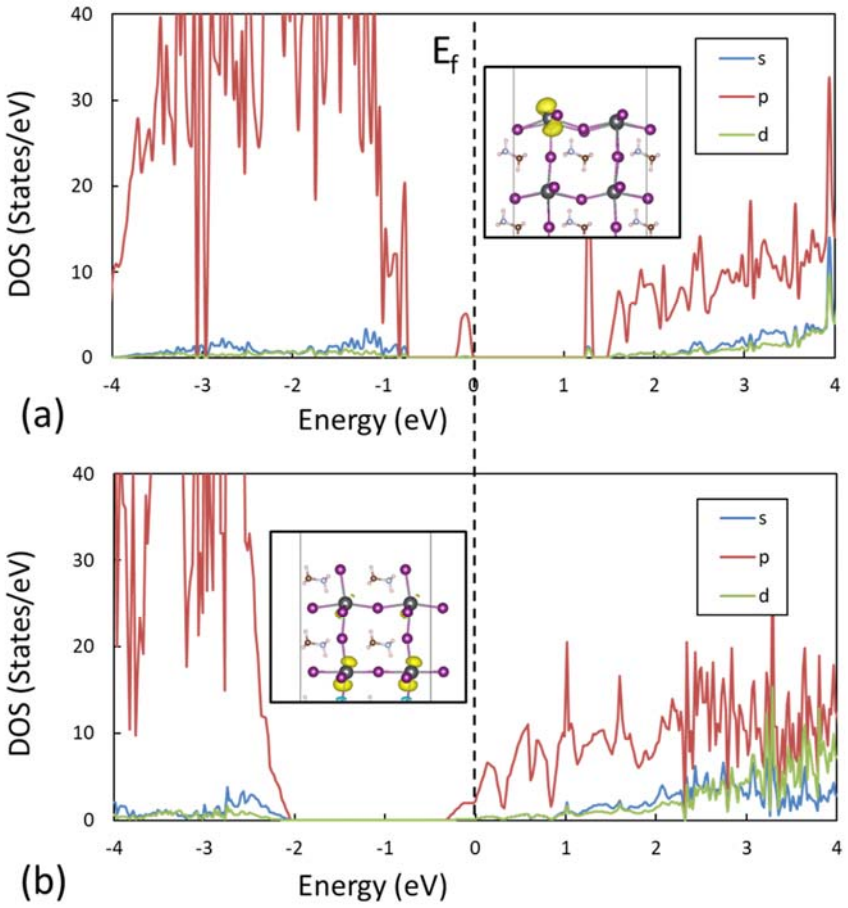

Figure 2. Density of states of (a) the PbI_2-terminated surface from electron localized calculations with SOC, and (b) the electron delocalized MAI-terminated surface with SOC, with the insert of the side view of the optimal structure. The Fermi level is set at 0 eV.

Considering that many photocatalytic reactions occur between the solid-liquid interphase[16, 20, 48], long AIMD simulations[49-51] were carried out to investigate both the MAI and PbI_2 terminated surfaces in the presence of HI solutions of varying concentrations. We find that all the surfaces were largely distorted due to the interactions between the surfaces and the solutions (Figure 3). Analyses of the average characteristic distances (average distance of four characteristic Pb-I bonds) from the whole AIMD simulations disclose remarkable differences on the two terminated

surfaces in a vacuum and in solutions. The average characteristic distances of MAI and PbI_2 terminations in a vacuum are 3.45 Å and 3.37 Å, respectively (Figure 1). However, the average characteristic distances of both terminations in the presence of the liquid phase (Table 1) are obviously longer than those in a vacuum. The average characteristic distance of MAI termination in the pure water is 3.96 Å, which is 0.2 - 0.3 Å longer than those in the HI solutions. As for the PbI_2 termination, the average characteristic distance is 4.00 Å in pure water, but with distances of 3.70, 3.71 and 3.77 Å in the HI solutions with the concentrations of 1.05 mol/L, 2.10 mol/L and 3.15 mol/L, respectively, similar to the trend observed from the MAI terminated surface. These results are consistent with the experimental observation that the $MAPbI_3$ perovskite is readily dissolved in the water, and yet the high concentration of aqueous HI solution can prevent the decomposition of the $MAPbI_3$ perovskite[16, 52]. The minimum concentration of the HI solution to keep $MAPbI_3$ solid is 3.162 mol/L in the previous experiment[16]. Interestingly, in our calculations, even in low concentrations of HI solution with only one HI molecule in the aqueous phase per unit cell (1.05 mol/L), the surface apparently becomes more stable than in the pure water. This result underpins the importance of the HI solution introduced for the stability of $MAPbI_3$ perovskite.

Table 1. Average distance between the Pb on the first layer PbI_2 and I below the first layer PbI_2. The unit of the concentrations is mol/L and the unit of the average distances is Å.

Concentration	Average distance	
	MAI-terminated	PbI_2-terminated
0	3.96	4.00
1.05	3.67	3.70
2.10	3.77	3.71
3.15	3.78	3.77

Having revealed the surface structure changes in the presence of HI solutions, it is worth discussing what effects they would cause on the electron localization. It is surprising to observe that not only the PbI_2 terminated surface, but also the MAI terminated surface can localize the electron in the presence of the liquid phase. As illustrated in Figure 3, whether in the pure water or in the HI solutions, the electron can always be trapped on a Pb site on the $MAPbI_3$(001) surfaces. The Bader charge differences of these electron-trapped Pb atoms are over 0.90 |e|, indicating that the excess charges are mainly localized on the Pb atom on the top layer of the surfaces. Moreover, by examining a number of snapshots in each AIMD simulations, we found that once the electron is trapped in the system, it will not be delocalized, indicating a good stability of the trapped state. It is worth emphasizing here that on the MAI terminated surface, the electron is delocalized in a vacuum, but it is localized in the presence of aqueous solutions. In addition, the local iodide ion diffusion was observed due to the surface structure distorted by the solutions. It was also discovered that the electron localization of the system would enhance the iodide ion migration, which was also observed in the previous works[53-54].

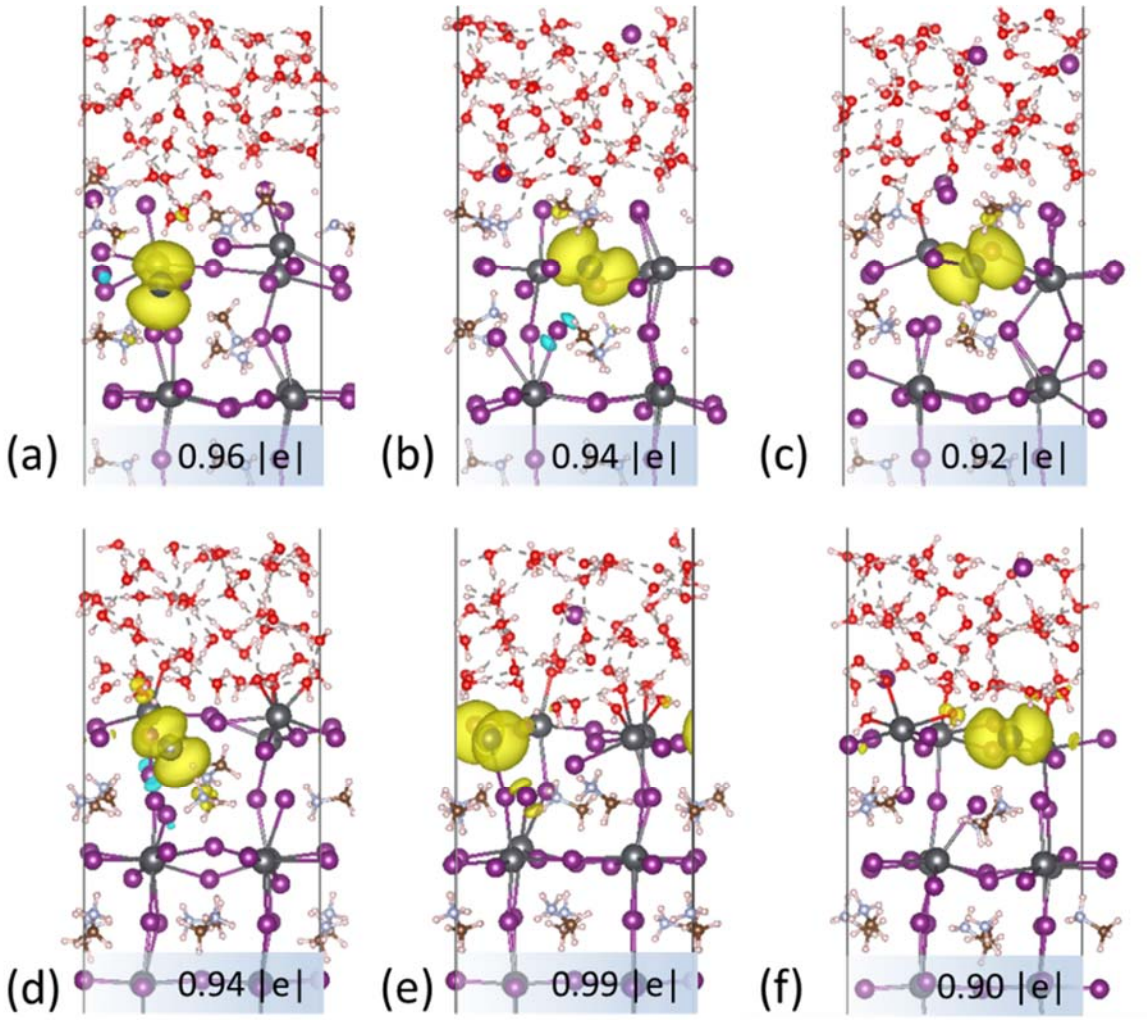

Figure 3. Geometric structures and spin densities of (a-c) MAI-terminated surfaces and (d-f) PbI_2-terminated surfaces in pure water ((a), (d)), 1.05 mol/L ((b), (e)), and 2.10 mol/L ((c), (f)) HI solutions with an extra electron. The iso-value is 0.001 e/Å^3. The Bader charge difference is illustrated in each structure.

In the real experimental condition, K^+ ions are present in the liquid phase. In some theoretical work, the system with an excess electron was simulated by adding a K atom in the water phase[55], in which the K atom becomes K^+ by losing an electron, resulting in an extra electron on the surface. In order to examine if the localized electronic state would be affected by different methods, we

added a K atom in our simulations. To be consistent with the experimental concentration of HI solution, 3.15 mol/L was chosen to be studied for the solid-liquid interface (Figure 4(a-d))[16]. Taking the PbI_2 terminated surface in the presence of HI solution with a K atom added (Figure 4(d)) as an example, we performed the following AIMD simulations. Firstly, the AIMD simulation was carried out, in which the liquid phase was relaxed with the surface slab fixed, until it reached the equilibrium plateau (~20 ps). Then, the system was fully relaxed except the bottom layer of the slab remaining being fixed. An additional AIMD simulation over 14 ps was performed; the system becomes thermodynamically stable after ~4 ps, and a further 10 ps AIMD simulation was conducted. One of the results from the simulation is shown in Figure 4(e) (more AIMD simulation results can be found in the Supporting Information). We notice that introducing the K atom would not affect the localization of the electronic states: The Bader charge differences of the Pb atoms with the localized electrons in the systems by adding K and adding an extra electron are almost the same, which are 0.94 and 0.92 |e| on the MAI terminated surface and 0.91 and 0.85 |e| on the PbI_2 terminated surface, respectively. This indicates that the feature of electron localization in the systems is independent of simulation methods.

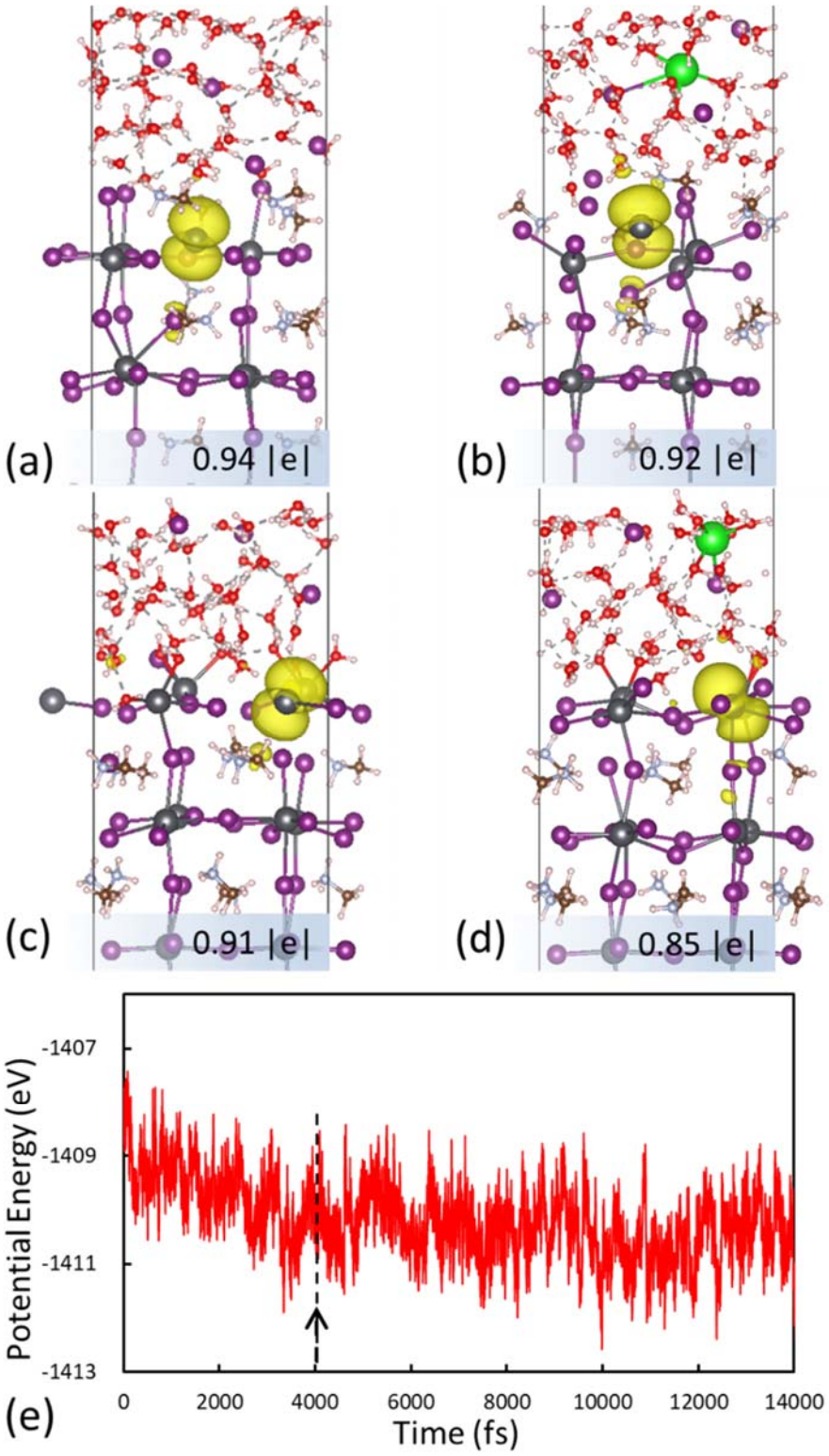
(a)
0.94 |e|
(b)
0.92 |e|
(c)
0.91 |e|
(d)
0.85 |e|
(e)
Potential Energy (eV)
-1407
-1409
-1411
-1413
0
2000
4000
6000
8000
10000
12000
14000
Time (fs)

Figure 4. Geometric structures and spin densities of (a)(b) MAI-terminated surfaces and (c)(d) PbI_2-terminated surfaces in 3.15 mol/L HI solution with an extra electron ((a), (c)) and a K atom ((b), (d)). The K atom is green. The iso-value is 0.001 e/Å^3. (e) Illustration of the energies of the system in (d) as a function of simulation time from an AIMD calculation as an example, while others are provided in the Supporting Information. The equilibration in AIMD occurs after ~4 ps as indicated by the arrow. The Bader charge difference is illustrated in each structure.

It is worth discussing the general trends of charge-localized structures. Comparing all the results presented here with the electron- and hole-localized structures in the other systems[24, 38, 56], we find that most of the charge-localized structures possess a feature of either a longer bond length or a broken bond (e.g. a Pb-I or Ti-O bond), at the metal site of which the electron is localized. In the bulk, the Pb atom bonds with six I atoms, creating an octahedron. Due to the stable Pb-I ligand in the bulk, it is difficult to trap an electron. In a vacuum, these two terminated surfaces display different Pb coordination; in the PbI_2 termination the penta-coordination of the electron-trapped Pb atom is unsaturated, whereas in the MAI termination, the coordination of Pb is saturated with each Pb atom coordinating with six I atoms. It is difficult to dissociate the Pb-I bond, forming a free iodide in a vacuum. Therefore, it is impossible for the electron to be trapped on the MAI-terminated surface in the absence of a liquid phase or adsorbates.

In the presence of the liquid phase, not only on the PbI_2 terminated surface but also the MAI terminated surface, the electron can be trapped. In contrast to the other Pb atoms that does not trap the electron in the MAI termination, the Pb atom with localized electron is not fully coordinated, which is featured by either the Pb-I bond weakening or breaking. Our AIMD simulations show that in the systems with the MAI termination in the liquid phase, the Pb-I bond breaking apparently occurs between the electron-trapped Pb atom and the I atom above it. Interestingly, in the PbI_2

terminated systems with the exception of the Pb atom with the localized electron, the other Pb atoms on the first layer are coordinated by one or two water molecules each. In other words, the other Pb atoms are in coordination with H_2O, while the Pb with a localized electron becomes inert for coordinating H_2O in the aqueous phase on the PbI_2 terminated surface. This further indicates that the electron can only be trapped on the unsaturated Pb atom. The I ion from the weakened Pb-I bond is precisely located at the interface between the MAI-terminated surface and the liquid phase, which enables it easily to bond with the water and form a hydrate iodide ion. The electron localization and the Pb-I bond breaking may occur in a concerted manner in real systems. This further indicates that the solutions or moisture would also promote the electron localization by distorting the surface, which may be a prerequisite to enhance the photocatalysis.

By examining all the structures from the AIMD simulations, we find that there may exist an intermediate surface, which is neither the MAI terminated surface nor the PbI_2 terminated one, shown in Figure S3. The MAI terminated surface can trap the electron after the coordinated I atom moves away in the presence of a solution. In an extreme scenario with four I atoms on the top layer removed, the MAI terminated surface will be transformed to a PbI_2 termination-like surface, on which a MA^+ cation layer remains, being exposed above the PbI_2 layer (Figure S3). This is an intermediate surface structure between the MAI and PbI_2 terminations. We find that this intermediate surface is also able to trap an extra electron; the electron localization on Pb atoms on the top layer of the surface is apparent, indicating that the MA^+ cation will not affect the electron-localized state. The apparently increased characteristic distances (Pb-I) are also observed in the system, as shown in Figure S3. This intermediate structure is unusual and to our knowledge, has not been reported before. It is worth stressing the importance of such a structure: Due to many photocatalytic reactions occurred in the liquid phase, the MA^+ cations on the top layer, located at

the interface between the liquid phase that supplies the protons[57] and the $MAPbI_3$ surface that provides the electrons, may play a key role in transferring the electron and proton in some reaction mechanisms[55]. This intermediate structure may be an important topic to be studied in the future.

Finally, it is worth mentioning the implications of our results. It is clear that the photogenerated electron localization is of great importance for the high efficiency of photovoltaic and photocatalytic materials[39]. However, it should also be noted that it is not desirable either if the electron is trapped in a local structure too deeply; the migration of the deeply trapped electron would be difficult. It is evident that defects can be local structures that trap the electrons[26, 29]. However, some defects, particularly the presence of several defects in a local area, may trap the electron too deeply. Thus, the delocalization of photogenerated electron and too deep electron trapping may be the two problems on the two sides of a volcano curve[58-60], respectively. Ideally, the photogenerated electron should be localized, but not trapped too deeply. To this end, the structure of PbI_2-terminated $MAPbI_3$ surface without defects may be a perfect location for the electron-trapping. One could envisage that the photogenerated electrons may first all move to the surface and then migrate to the right sites for photovoltaic or photocatalytic processes. In addition, our work may provide some insight into the humidity issue in $MAPbI_3$ perovskite systems. Some moistures may facilitate the electron trapping; on the other hand, too much water may dissolve $MAPbI_3$, creating too many defects, which is not desirable either, as demonstrated in our work.

In summary, we systematically investigated the localization of photo-generated electrons in the bulk of $MAPbI_3$ and on the stochiometric $MAPbI_3$(001) surfaces in a vacuum as well as in the presence of liquid phases, using high level first-principles calculations. We showed that the electron cannot be localized in the bulk of $MAPbI_3$ but can be trapped on a defect-free $MAPbI_3$(001) surface. Our work demonstrated that the electron localization always occurs in the

system with the Pb-I bond weakened or broken. For the bulk of $MAPbI_3$ and the $MAPbI_3$(001) surface in the MAI termination in a vacuum, the coordination number of Pb atom is fully saturated, resulting in the electron delocalization in the systems. In contrast, the Pb atom on the PbI_2-terminated surface lacks a ligand I atom, leading it more liable to trap the electron. The AIMD calculations illustrated that the presence of HI solutions with different concentrations will prompt the deformation of the $MAPbI_3$(001) surfaces such that they can localize the electrons on both the MAI and PbI_2 terminated surfaces. Furthermore, we observed an unusual intermediate surface structure between the MAI and PbI_2 terminations, which may possess a high activity in photocatalytic reactions.

ASSOCIATED CONTENT

Supporting Information

The Supporting Information is available free of charge on the ACS Publications website at DOI: XXXX

Analysis of spin densities and density of states, molecular dynamics simulations, computational details, calculation scheme for different concentrations of HI solutions

AUTHOR INFORMATION

Corresponding Authors

Peijun Hu - School of Chemistry and Chemical Engineering, The Queen's University of Belfast, Belfast, BT9 5AG, UK; Email: p.hu@qub.ac.uk

Meilan Huang - School of Chemistry and Chemical Engineering, The Queen's University of Belfast, Belfast, BT9 5AG, UK; Email: m.huang@qub.ac.uk.

Authors

Yunxuan Ding - School of Chemistry and Chemical Engineering, The Queen's University of Belfast, Belfast, BT9 5AG, UK

Yujie Shen - School of Chemistry and Chemical Engineering, The Queen's University of Belfast, Belfast, BT9 5AG, UK

Chao Peng - School of Chemistry and Chemical Engineering, The Queen's University of Belfast, Belfast, BT9 5AG, UK

Notes

The authors declare no competing financial interests.

ACKNOWLEDGMENT

The authors gratefully acknowledge the UK's national high performance computing service ARCHER, THOMAS and QUB high performance computing centre for computing resources. Y.X.D. thanks the Queen's University Belfast and China Scholarship Council for the PhD studentship. C.P. thanks the National Science Foundation of Hunan Province (2019JJ50526).

REFERENCES

(1). Brenner, T. M.; Egger, D. A.; Kronik, L.; Hodes, G.; Cahen, D. Hybrid organic-inorganic perovskites: low-cost semiconductors with intriguing charge-transport properties. *Nat. Rev. Mater.* **2016**, *1*, 15007.

(2). Green, M. A.; Ho-Baillie, A.; Snaith, H. J. The emergence of perovskite solar cells. *Nat. Photonics* **2014**, *8*, 506-514.

(3). Li, N.; Tao, S.; Chen, Y.; Niu, X.; Onwudinanti, C. K.; Hu, C.; Qiu, Z.; Xu, Z.; Zheng, G.; Wang, L.; *et al.* Cation and anion immobilization through chemical bonding enhancement with fluorides for stable halide perovskite solar cells. *Nat. Energy* **2019**, *4*, 408-415.

(4). Kojima, A.; Teshima, K.; Shirai, Y.; Miyasaka, T. Organometal halide perovskites as visible-light sensitizers for photovoltaic cells. *J. Am. Chem. Soc.* **2009**, *131*, 6050-6051.

(5). Im, J. H.; Lee, C. R.; Lee, J. W.; Park, S. W.; Park, N. G. 6.5% efficient perovskite quantum-dot-sensitized solar cell. *Nanoscale* **2011**, *3*, 4088-4093.

(6). Jeon, N. J.; Noh, J. H.; Yang, W. S.; Kim, Y. C.; Ryu, S.; Seo, J.; Seok, S. I. Compositional engineering of perovskite materials for high-performance solar cells. *Nature* **2015**, *517*, 476-480.

(7). Park, N.-G.; Grätzel, M.; Miyasaka, T.; Zhu, K.; Emery, K. Towards stable and commercially available perovskite solar cells. *Nat. Energy* **2016**, *1*, 16152.

(8). Yang, W. S.; Park, B. W.; Jung, E. H.; Jeon, N. J.; Kim, Y. C.; Lee, D. U.; Shin, S. S.; Seo, J.; Kim, E. K.; Noh, J. H.; *et al.* Iodide management in formamidinium-lead-halide-based perovskite layers for efficient solar cells. *Science* **2017**, *356*, 1376-1379.

(9). Kim, J. Y.; Lee, J. W.; Jung, H. S.; Shin, H.; Park, N. G. High-Efficiency Perovskite Solar Cells. *Chem. Rev.* **2020**, *120*, 7867-7918.

(10). Redondo-Obispo, C.; Suarez, I.; Quesada, S. J.; Ripolles, T. S.; Martinez-Pastor, J. P.; Alvarez, A. L.; de Andres, A.; Coya, C. Enhanced Nonlinear Optical Coefficients of $MAPbI_3$ Thin Films by Bismuth Doping. *J. Phys. Chem. Lett.* **2020**, *11*, 2188-2194.

(11). Ong, K. P.; Wu, S.; Nguyen, T. H.; Singh, D. J.; Fan, Z.; Sullivan, M. B.; Dang, C. Multi Band Gap Electronic Structure in $CH_3NH_3PbI_3$. *Sci. Rep.* **2019**, *9*, 2144.

(12). Lim, J.; Hörantner, M. T.; Sakai, N.; Ball, J. M.; Mahesh, S.; Noel, N. K.; Lin, Y.-H.; Patel, J. B.; McMeekin, D. P.; Johnston, M. B.; *et al.* Elucidating the long-range charge carrier mobility in metal halide perovskite thin films. *Energy Environ. Sci.* **2019**, *12*, 169-176.

(13). Shi, D.; Adinolfi, V.; Comin, R.; Yuan, M.; Alarousu, E.; Buin, A.; Chen, Y.; Hoogland, S.; Rothenberger, A.; Katsiev, K.; *et al.* Solar cells. Low trap-state density and long carrier diffusion in organolead trihalide perovskite single crystals. *Science* **2015**, *347*, 519-522.

(14). Dong, Q.; Fang, Y.; Shao, Y.; Mulligan, P.; Qiu, J.; Cao, L.; Huang, J. Solar cells. Electron-hole diffusion lengths > 175 mum in solution-grown $CH_3NH_3PbI_3$ single crystals. *Science* **2015**, *347*, 967-970.

(15). Galkowski, K.; Mitioglu, A.; Miyata, A.; Plochocka, P.; Portugall, O.; Eperon, G. E.; Wang, J. T.-W.; Stergiopoulos, T.; Stranks, S. D.; Snaith, H. J.; *et al.* Determination of the exciton binding energy and effective masses for methylammonium and formamidinium lead tri-halide perovskite semiconductors. *Energy Environ. Sci.* **2016**, *9*, 962-970.

(16). Park, S.; Chang, W. J.; Lee, C. W.; Park, S.; Ahn, H.-Y.; Nam, K. T. Photocatalytic hydrogen generation from hydriodic acid using methylammonium lead iodide in dynamic equilibrium with aqueous solution. *Nat. Energy* **2016**, *2*, 16185.

(17). Wu, Y.; Wang, P.; Zhu, X.; Zhang, Q.; Wang, Z.; Liu, Y.; Zou, G.; Dai, Y.; Whangbo, M. H.; Huang, B. Composite of $CH_3NH_3PbI_3$ with Reduced Graphene Oxide as a Highly Efficient and

Stable Visible-Light Photocatalyst for Hydrogen Evolution in Aqueous HI Solution. *Adv. Mater.* **2018**, *30*, 1704342.

(18). Kim, D.; Lee, D. K.; Kim, S. M.; Park, W.; Sim, U. Photoelectrochemical Water Splitting Reaction System Based on Metal-Organic Halide Perovskites. *Materials* **2020**, *13*, 210.

(19). Xu, Y. F.; Yang, M. Z.; Chen, B. X.; Wang, X. D.; Chen, H. Y.; Kuang, D. B.; Su, C. Y. A $CsPbBr_3$ Perovskite Quantum Dot/Graphene Oxide Composite for Photocatalytic CO_2 Reduction. *J. Am. Chem. Soc.* **2017**, *139*, 5660-5663.

(20). Wu, L. Y.; Mu, Y. F.; Guo, X. X.; Zhang, W.; Zhang, Z. M.; Zhang, M.; Lu, T. B. Encapsulating Perovskite Quantum Dots in Iron-Based Metal-Organic Frameworks (MOFs) for Efficient Photocatalytic CO_2 Reduction. *Angew. Chem. Int. Ed.* **2019**, *58*, 9491-9495.

(21). Peng, C.; Reid, G.; Wang, H.; Hu, P. Perspective: Photocatalytic reduction of CO_2 to solar fuels over semiconductors. *J. Chem. Phys.* **2017**, *147*, 030901.

(22). Fu, J.; Liu, K.; Jiang, K.; Li, H.; An, P.; Li, W.; Zhang, N.; Li, H.; Xu, X.; Zhou, H.; *et al.* Graphitic Carbon Nitride with Dopant Induced Charge Localization for Enhanced Photoreduction of CO_2 to CH_4. *Adv. Sci.* **2019**, *6*, 1900796.

(23). Li, J.; Dong, X. a.; Sun, Y.; Jiang, G.; Chu, Y.; Lee, S. C.; Dong, F. Tailoring the rate-determining step in photocatalysis via localized excess electrons for efficient and safe air cleaning. *Appl. Catal. B* **2018**, *239*, 187-195.

(24). Wang, D.; Sheng, T.; Chen, J.; Wang, H. F.; Hu, P. Identifying the key obstacle in photocatalytic oxygen evolution on rutile TiO_2. *Nat. Catal.* **2018**, *1*, 291-299.

(25). Wang, D.; Li, F.; Chen, J.-F.; Wang, H.-F.; Cao, X.-M.; Hu, P.; Gong, X.-Q. Computational Simulation of Trapped Charge Carriers in TiO_2 and Their Impacts on Photocatalytic Water Splitting. *ACS Symp. Ser.* **2019**, *1331*, 67-100.

(26). Qiao, L.; Fang, W. H.; Long, R. The Interplay between Lead Vacancy and Water Rationalizes the Puzzle of Charge Carrier Lifetimes in $CH_3NH_3PbI_3$: Time-Domain Ab Initio Analysis. *Angew. Chem. Int. Ed.* **2020**, *59*, 13347.

(27). Long, R.; Liu, J.; Prezhdo, O. V. Unravelling the Effects of Grain Boundary and Chemical Doping on Electron-Hole Recombination in $CH_3NH_3PbI_3$ Perovskite by Time-Domain Atomistic Simulation. *J. Am. Chem. Soc.* **2016**, *138*, 3884-3890.

(28). Jankowska, J.; Long, R.; Prezhdo, O. V. Quantum Dynamics of Photogenerated Charge Carriers in Hybrid Perovskites: Dopants, Grain Boundaries, Electric Order, and Other Realistic Aspects. *ACS Energy Lett.* **2017**, *2*, 1588-1597.

(29). Li, W.; Long, R.; Tang, J.; Prezhdo, O. V. Influence of Defects on Excited-State Dynamics in Lead Halide Perovskites: Time-Domain ab Initio Studies. *J. Phys. Chem. Lett.* **2019**, *10*, 3788-3804.

(30). Yang, J.; Wang, D.; Han, H.; Li, C. Roles of cocatalysts in photocatalysis and photoelectrocatalysis. *Acc. Chem. Res.* **2013**, *46*, 1900-1909.

(31). Ma, Y.; Wang, X.; Jia, Y.; Chen, X.; Han, H.; Li, C. Titanium dioxide-based nanomaterials for photocatalytic fuel generations. *Chem. Rev.* **2014**, *114*, 9987-10043.

(32). Hisatomi, T.; Kubota, J.; Domen, K. Recent advances in semiconductors for photocatalytic and photoelectrochemical water splitting. *Chem. Soc. Rev.* **2014**, *43*, 7520-7535.

(33). Peng, C.; Wang, J.; Wang, H.; Hu, P. Unique Trapped Dimer State of the Photogenerated Hole in Hybrid Orthorhombic $CH_3NH_3PbI_3$ Perovskite: Identification, Origin, and Implications. *Nano Lett.* **2017**, *17*, 7724-7730.

(34). Peng, C.; Chen, J.; Wang, H.; Hu, P. First-Principles Insight into the Degradation Mechanism of $CH_3NH_3PbI_3$ Perovskite: Light-Induced Defect Formation and Water Dissociation. *J. Phys. Chem. C* **2018**, *122*, 27340-27349.

(35). Samu, G. F.; Balog, A.; De Angelis, F.; Meggiolaro, D.; Kamat, P. V.; Janaky, C. Electrochemical Hole Injection Selectively Expels Iodide from Mixed Halide Perovskite Films. *J. Am. Chem. Soc.* **2019**, *141*, 10812-10820.

(36). Uratani, H.; Yamashita, K. Charge Carrier Trapping at Surface Defects of Perovskite Solar Cell Absorbers: A First-Principles Study. *J. Phys. Chem. Lett.* **2017**, *8*, 742-746.

(37). Wang, J.; Li, W.; Yin, W. J. Passivating Detrimental DX Centers in $CH_3NH_3PbI_3$ for Reducing Nonradiative Recombination and Elongating Carrier Lifetime. *Adv. Mater.* **2020**, *32*, 1906115.

(38). Che, X.; Traore, B.; Katan, C.; Fang, H.-H.; Loi, M. A.; Even, J.; Kepenekian, M. Charge Trap Formation and Passivation in Methylammonium Lead Tribromide. *J. Phys. Chem. C* **2019**, *123*, 13812-13817.

(39). Ambrosio, F.; Meggiolaro, D.; Mosconi, E.; De Angelis, F. Charge localization and trapping at surfaces in lead-iodide perovskites: the role of polarons and defects. *J. Mater. Chem. A* **2020**, *8*, 6882-6892.

(40). Zhang, L.; Sit, P. H. L. Ab initio study of the dynamics of electron trapping and detrapping processes in the $CH_3NH_3PbI_3$ perovskite. *J. Mater. Chem. A* **2019**, *7*, 2135-2147.

(41). Taufique, M. F. N.; Khanal, R.; Choudhury, S.; Banerjee, S. Impact of iodine antisite (IPb) defects on the electronic properties of the (110) $CH_3NH_3PbI_3$ surface. *J. Chem. Phys.* **2018**, *149*, 164704.

(42). Bregante, D. T.; Johnson, A. M.; Patel, A. Y.; Ayla, E. Z.; Cordon, M. J.; Bukowski, B. C.; Greeley, J.; Gounder, R.; Flaherty, D. W. Cooperative Effects between Hydrophilic Pores and Solvents: Catalytic Consequences of Hydrogen Bonding on Alkene Epoxidation in Zeolites. *J. Am. Chem. Soc.* **2019**, *141*, 7302-7319.

(43). Zeng, Z.; Greeley, J. Characterization of oxygenated species at water/Pt(111) interfaces from DFT energetics and XPS simulations. *Nano Energy* **2016**, *29*, 369-377.

(44). Sun, X.; Wang, P.; Shao, Z.; Cao, X.; Hu, P. A first-principles microkinetic study on the hydrogenation of carbon dioxide over Cu(211) in the presence of water. *Sci. China Chem.* **2019**, *62*, 1686-1697.

(45). Zhou, H.; Chen, Q.; Li, G.; Luo, S.; Song, T. B.; Duan, H. S.; Hong, Z.; You, J.; Liu, Y.; Yang, Y. Photovoltaics. Interface engineering of highly efficient perovskite solar cells. *Science* **2014**, *345*, 542-546.

(46). Christians, J. A.; Miranda Herrera, P. A.; Kamat, P. V. Transformation of the excited state and photovoltaic efficiency of $CH_3NH_3PbI_3$ perovskite upon controlled exposure to humidified air. *J. Am. Chem. Soc.* **2015**, *137*, 1530-1538.

(47). Eperon, G. E.; Habisreutinger, S. N.; Leijtens, T.; Bruijnaers, B. J.; van Franeker, J. J.; deQuilettes, D. W.; Pathak, S.; Sutton, R. J.; Grancini, G.; Ginger, D. S.*; et al.* The Importance of Moisture in Hybrid Lead Halide Perovskite Thin Film Fabrication. *ACS Nano* **2015**, *9*, 9380-9393.

(48). Zhu, X.; Lin, Y.; San Martin, J.; Sun, Y.; Zhu, D.; Yan, Y. Lead halide perovskites for photocatalytic organic synthesis. *Nat. Commun.* **2019**, *10*, 2843.

(49). Wang, D.; Liu, Z.-P.; Yang, W.-M. Proton-Promoted Electron Transfer in Photocatalysis: Key Step for Photocatalytic Hydrogen Evolution on Metal/Titania Composites. *ACS Catal.* **2017**, *7*, 2744-2752.

(50). Wang, D.; Liu, Z.-P.; Yang, W.-M. Revealing the Size Effect of Platinum Cocatalyst for Photocatalytic Hydrogen Evolution on TiO_2 Support: A DFT Study. *ACS Catal.* **2018**, *8*, 7270-7278.

(51). Rice, P. S.; Mao, Y.; Guo, C.; Hu, P. Interconversion of hydrated protons at the interface between liquid water and platinum. *Phys. Chem. Chem. Phys.* **2019**, *21*, 5932-5940.

(52). Mosconi, E.; Azpiroz, J. M.; De Angelis, F. Ab Initio Molecular Dynamics Simulations of Methylammonium Lead Iodide Perovskite Degradation by Water. *Chem. Mater.* **2015**, *27*, 4885-4892.

(53). Wen, X.; Ho-Baillie, A.; Huang, S.; Sheng, R.; Chen, S.; Ko, H. C.; Green, M. A. Mobile Charge-Induced Fluorescence Intermittency in Methylammonium Lead Bromide Perovskite. *Nano Lett.* **2015**, *15*, 4644-4649.

(54). Gottesman, R.; Gouda, L.; Kalanoor, B. S.; Haltzi, E.; Tirosh, S.; Rosh-Hodesh, E.; Tischler, Y.; Zaban, A.; Quarti, C.; Mosconi, E.; *et al.* Photoinduced Reversible Structural Transformations in Free-Standing $CH_3NH_3PbI_3$ Perovskite Films. *J. Phys. Chem. Lett.* **2015**, *6*, 2332-2338.

(55). Wang, L.; Xiao, H.; Cheng, T.; Li, Y.; Goddard, W. A., 3rd Pb-Activated Amine-Assisted Photocatalytic Hydrogen Evolution Reaction on Organic-Inorganic Perovskites. *J. Am. Chem. Soc.* **2018**, *140*, 1994-1997.

(56). Zhang, J.; Peng, C.; Wang, H.; Hu, P. Identifying the Role of Photogenerated Holes in Photocatalytic Methanol Dissociation on Rutile TiO_2(110). *ACS Catal.* **2017**, *7*, 2374-2380.

(57). Li, N.; Ding, Y.; Wu, J.; Zhao, Z.; Li, X.; Zheng, Y. Z.; Huang, M.; Tao, X. Efficient, Full Spectrum-Driven H_2 Evolution Z-Scheme Co_2P/CdS Photocatalysts with Co-S Bonds. *ACS Appl. Mater. Interfaces* **2019**, *11*, 22297-22306.

(58). Wang, Z.; Hu, P. Identifying the general trend of activity of non-stoichiometric metal oxide phases for CO oxidation on Pd(111). *Sci. China Chem.* **2019**, *62*, 784-789.

(59). Ding, Y.; Xu, Y.; Mao, Y.; Wang, Z.; Hu, P. Achieving rational design of alloy catalysts using a descriptor based on a quantitative structure-energy equation. *Chem. Commun.* **2020**, *56*, 3214-3217.

(60). Ding, Y.; Xu, Y.; Song, Y.; Guo, C.; Hu, P. Quantitative Studies of the Coverage Effects on Microkinetic Simulations for NO Oxidation on Pt(111). *J. Phys. Chem. C* **2019**, *123*, 27594-27602.